JACS
JOURNAL OF THE AMERICAN CHEMICAL SOCIETY
pubs.acs.org/JACS
Communication

Fluorescence-Detected Mid-Infrared Photothermal Microscopy

Minghe Li,[‖] Aleksandr Razumtcev,[‖] Ruochen Yang, Youlin Liu, Jiayue Rong, Andreas C. Geiger, Romain Blanchard, Christian Pfluegl, Lynne S. Taylor, and Garth J. Simpson*

Cite This: J. Am. Chem. Soc. 2021, 143, 10809−10815
Read Online
ACCESS | Metrics & More | Article Recommendations | Supporting Information

ABSTRACT: We demonstrate instrumentation and methods to enable fluorescence-detected photothermal infrared (F-PTIR) microscopy and then demonstrate the utility of F-PTIR to characterize the composition within phase-separated domains of model amorphous solid dispersions (ASDs) induced by water sorption. In F-PTIR, temperature-dependent changes in fluorescence quantum efficiency are shown to sensitively report on highly localized absorption of mid-infrared radiation. The spatial resolution with which infrared spectroscopy can be performed is dictated by fluorescence microscopy, rather than the infrared wavelength. Intrinsic ultraviolet autofluorescence of tryptophan and protein microparticles enabled label-free F-PTIR microscopy. Following proof of concept F-PTIR demonstration on model systems of polyethylene glycol (PEG) and silica gel, F-PTIR enabled the characterization of chemical composition within inhomogeneous ritonavir/polyvinylpyrrolidone-vinyl acetate (PVPVA) amorphous dispersions. Phase separation is implicated in the observation of critical behaviors in ASD dissolution kinetics, with the results of F-PTIR supporting the formation of phase-separated drug-rich domains upon water sorption in spin-cast films.

Photothermal infrared microscopy has recently emerged as a powerful tool for high-resolution optical imaging, with numerous advantages relative to alternative methods for pharmaceutical materials analysis. Photothermal microscopy with a spatial resolution on the order of a few nanometers has been realized by photothermal atomic force microscopy infrared spectroscopy (AFM-IR),[1,2] in which heat-induced perturbation to an atomic force microscope tip informs on surface absorption. Photothermal AFM-IR is now a mature technology, routinely capable of providing mid-infrared microspectroscopy with nanometer-scale spatial resolution,[3] with growing use in analysis of pharmaceutically relevant materials.[4] However, it suffers from two key limitations; (i) like most scanning probe microscopy methods, the mechanical response time of the cantilever sets a practical speed limit on pixel and frame rates, often requiring several minutes for a single image, and (ii) by design, it intrinsically can only inform on absorption in the region immediately adjacent to the surface.

Several of the limitations of photothermal AFM-IR can be overcome by using light to transduce the photothermal temperature change. In optically detected photothermal infrared (O-PTIR), subtle changes in refractive index induced by local temperature changes from absorption of an IR beam are recorded through perturbation of a co- or counter-propagating visible beam.[5,6] For pharmaceutical materials analysis, O-PTIR has been used by Li et al. in an epi-detection configuration compatible with analysis of powders and opaque solid-state materials.[7] In brief, a mid-infrared beam from a quantum cascade laser (QCL) was copropagated with a 785 nm visible beam using a reflective Cassegrain objective. IR-induced modulation in the backscattered visible light was detected using a polarizing beam-splitting cube, exploiting depolarization by the highly turbid solid-state samples. IR-modulated changes in the backscattering enabled spectral assignment of active and inactive ingredients in a Tylenol tablet.

Despite these successes, O-PTIR measured by perturbation of a probe beam suffers from several limitations, exacerbated in analysis of pharmaceutical materials. First, refractive index is a fairly weak function of temperature, changing by ∼0.01% per °C for water at room temperature.[8] Second, it is well-known that the photothermally induced deflection of a probe beam in transmission approaches zero for a point source centered in the probe beam focus and is maximized with an axial offset between the probe beam and photothermal lens of $\sqrt{3}Z_0$ (Z_0 is the Rayleigh range, equal to half the depth of focus).[9,10] As such, an O-PTIR measurement of a point source along the optical axis based on detection of beam deflection is only expected to produce peak signals in homogeneous media when the probe beam focus is displaced by nearly a full depth of field relative to the photothermal source, potentially producing nontrivial 3D point spread functions.

For measurements of transparent samples acquired in transmission, this limitation can be overcome by coupling O-PTIR with quantitative phase contrast approaches, such as those developed by Popescu and co-workers,[12−14] enabling photothermal contrast through interferometry rather than beam deflection.[15] Dual-path interferometric approaches have also been shown by Orrit and co-workers to enable sensitive

Received: March 28, 2021
Published: July 16, 2021

https://doi.org/10.1021/jacs.1c03269
J. Am. Chem. Soc. 2021, 143, 10809−10815

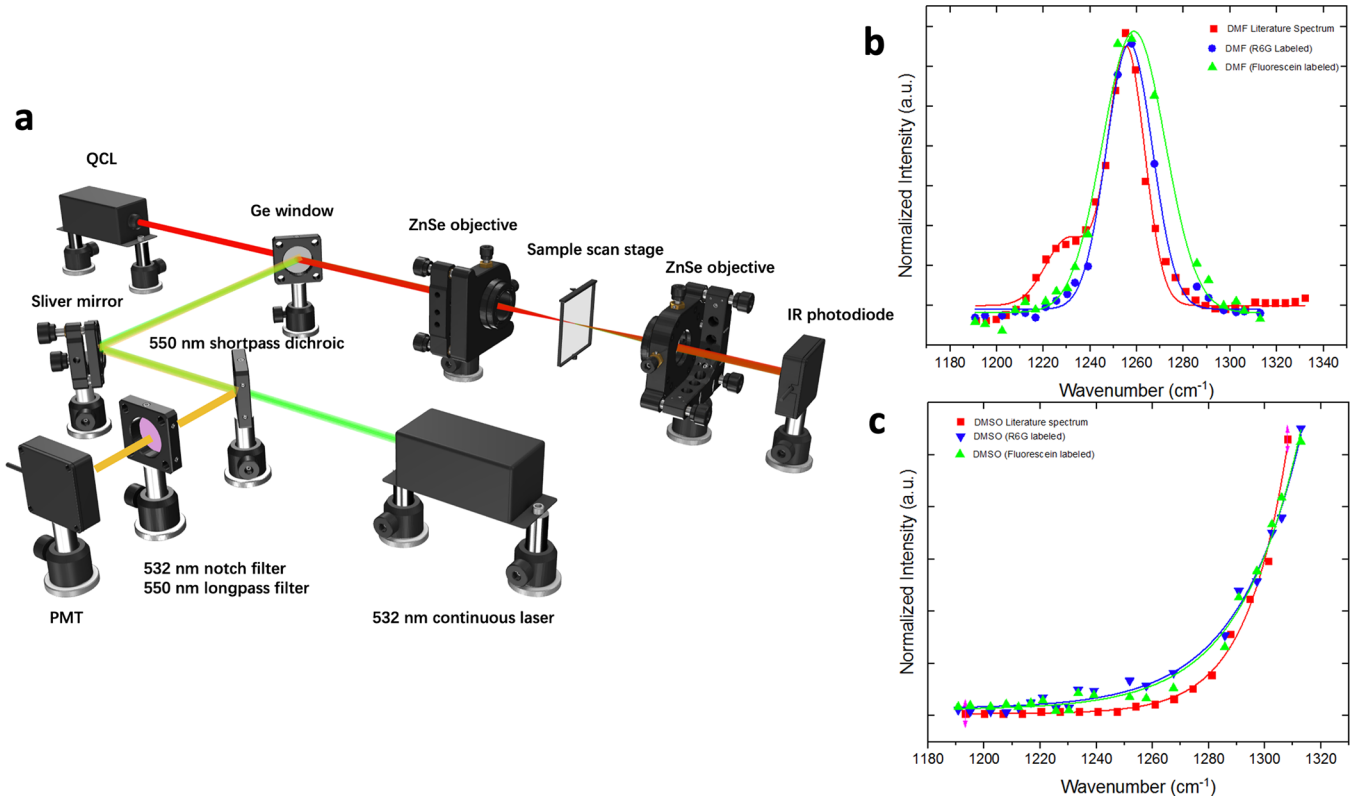

Figure 1. (a) F-PTIR microscope configuration. (b and c) A comparison between IR spectra of DMF and DMSO recovered using F-PTIR with the literature data[11] for measurements performed with R6G and fluorescein as fluorophores. The dye concentration was 2.1 mM for R6G and 3 mM for fluorescein.

photothermal visible-wavelength absorption spectroscopy of particles in solution, approaching single molecule sensitivity.[16] However, many pharmaceutical materials exhibit significant turbidity and heterogeneity, creating challenges for analytically modeling and interpreting photothermal changes in back-scattered intensity from chemically and physically heterogeneous samples. In many instances, the optical constants associated with temperature change are not known, complicating quantitative interpretation of the magnitude of O-PTIR responses. Furthermore, the detected backscattered signal can depend on both depolarization and scattering in ways that may depend nontrivially on the particle size distribution within compacted or powdered samples.

An alternative optical method for thermal reporting may provide complementary advantages to current strategies based on refractive index detection. In particular, we explore herein the potential viability of using fluorescence intensity to detect local changes in temperature induced by mid-infrared absorption. The quantum efficiency of fluorescence is well established to vary sensitively with temperature.[17] Following optical excitation, increases in temperature enable access to a greater suite of thermally accessible relaxation pathways, all of which compete with fluorescence for a net reduction in fluorescence intensity. Temperature-dependent changes in autofluorescence emission have been reported in microscale thermophoresis, which target measurements of protein mobility and thermal stability.[18−21] In related work, Gruebele and co-workers have used the temperature-dependence of both native autofluorescence[22] and labeled fluorescence[23,24] to recover time scales for protein dynamics in temperature-jump experiments.

Compared to refractive index changes, the change in fluorescence quantum efficiency can be quite large, routinely changing by ∼2−3%/°C for tryptophan[25] and ∼1−2%/°C for aqueous solutions of rhodamine B,[26] corresponding to an ∼100-fold higher relative change than refractive index detection. Given the high signal-to-noise with which fluorescence measurements are regularly recorded, this sensitivity has the potential to be more than sufficient to enable fluorescence detection of local temperature perturbations of <1 °C induced by mid-infrared absorption.

The F-PTIR implementation developed herein is distinct from prior studies on fluorescence encoded IR (FEIR) by Tokmakoff and co-workers,[27] based on IR+Vis two-photon excited fluorescence. In FEIR spectroscopy, the infrared absorber must necessarily be energetically coupled to the electronic transition to support coherent two photon absorption, with corresponding improvements in selectivity for particular fluorophores of interest. As such, FEIR provides information on strongly coupled vibrational modes (e.g., those within the fluorophore molecular frame). In contrast to FEIR, the excitation pulses used in F-PTIR (>100 ns) are much longer than vibrational coherence and relaxation times in condensed phase media (typically a few picoseconds). As such, image contrast is squarely dominated by thermalization of the infrared excitation within the bath surrounding the reporting fluorophores.

While the primary focus of the present study is on qualitative determination of composition, quantification of local analyte concentration by F-PTIR has the potential to be influenced by the local microenvironment. Many fluorophores exhibit changes in quantum yield in hydrophilic vs hydrophobic

https://doi.org/10.1021/jacs.1c03269
J. Am. Chem. Soc. 2021, 143, 10809−10815

environments, which also suggests potential for differences in sensitivity in quantum efficiency with temperature (i.e., dQE/dT). Previous protein folding studies suggest minor or negligible changes in dQE/dT following denaturation and corresponding exposure of fluorophores to hydrophobic domains.[20] For comparison, the temperature-dependence of refractive index in O-PTIR (dn/dT) can vary by 340% between lipid-rich[28] vs aqueous[29] systems.

It is worth noting that O-PTIR and F-PTIR are not mutually exclusive; both can in principle be performed simultaneously. When using fluorescent labeling in optical microscopy, the labeled species are typically the most scientifically relevant, with F-PTIR providing additional information on the local environment immediately adjacent to a region of interest identified by fluorescence. In contrast, O-PTIR can inform broadly on local composition.

F-PTIR has the potential to be particularly advantageous for samples in which the reporting fluorophores are colocalized within the IR-absorbing regions of interest, either through targeted labeling or preferential partitioning. Simulations of the temperature distribution during and following IR absorption for a subdiffraction limited point source are detailed in the Supporting Information, along with the predicted O-PTIR and F-PTIR responses. These results suggest colocalization can provide ∼100-fold additional increases in signal-to-noise relative to noncolocalized F-PTIR, with much faster onset and relaxation times supporting high speed optical modulation. The higher sensitivity from fast onset/relaxation times suggests F-PTIR should support preferential interrogation of the absorption in the region immediately adjacent to the probe fluorophore, enabling site-specific vibrational spectroscopy through targeted fluorescence labeling.

Following initial proof-of-concept measurement supporting the viability of fluorescence-detected photothermal infrared (F-PTIR) microscopy, we demonstrate its utility in unambiguous observation of water-induced amorphous/amorphous phase separation (AAPS) in amorphous solid dispersions of ritonavir in poly(vinylpyrrolidone/vinyl acetate) (PVPVA), with direct implications in pharmaceutical materials design.

The F-PTIR microscope consisted of a 532 nm green laser (SLOC Lasers for continuous wave, Fianium Femtopower1060 for ultrafast) copropagating with a broadly tunable QCL array (Pendar Technologies) (Figure 1A). The average power of the green laser was around 0.2 mW on the sample plane for rhodamine-6G (R6G) associated samples and 30 mW for samples associated with Nile red as the fluorescent reporter. The monolithic QCL included 32 independently addressable wavelength channels in the range of wavenumbers from 1190 to 1330 cm^{-1}.[30] In typical operation, the QCL array was operated in a burst mode, in which a rapid series of 300 ns laser pulses was sequentially activated firing every 8 μs for "on" cycles ranging from 20 to 250 μs, followed by quiescent "off" periods of equal duration, with an average power of ≤0.8 mW on the sample plane. Timing details are described in greater detail in the Supporting Information. The net duty cycle of the QCL in this mode was maintained at <2% overall in single wavelength mode and ∼4−5% for multichannel operation.

The visible and mid-IR lasers were focused to the sample plane through a zinc selenide (ZnSe) lens (f = 25 mm, Thorlabs), calibrated using a clear pass USAF test grid (Edmund Optics). Divergence of the QCL beam was adjusted to align the visible and infrared focal planes. Images were collected by sample scanning with a piezoelectric stage (MadCityLabs Nano-BIO300). A photomultiplier tube (PMT, Hamamatsu) was used to collect the fluorescence signal from the sample in epi-configuration. A 532 nm notch filter and a 550 nm long pass filter were used to block the incident 532 nm light in front of the PMT. Signal from the PMT was passed through a tunable electronic band-pass filter (Ithaco M4302) centered at the QCL modulation frequency. The frequency-filtered signal was then passed through the lock-in amplifier (Stanford Research SR810). The de-modulated signal was then digitized (Alazar ATS9462), with images generated using MATLAB software written in-house. For spectral acquisition, F-PTIR signals for each wavelength channel were normalized to the transmitted intensity in the absence of a sample measured using an IR-photodiode (VIGO Systems).

Prior to implementation in microscopy, F-PTIR and FTIR spectra for thin liquid films were compared in Figure 1B and C. As can be seen in the figure, the F-PTIR spectra were generally in good agreement with infrared absorbance spectra of both DMF and DMSO within the wavelength range accessible by the QCL and independent of the fluorophore (R6G and fluorescein).

Silica gel particles served to assess characteristics of the F-PTIR microscope, the results of which are shown in Figure 2.

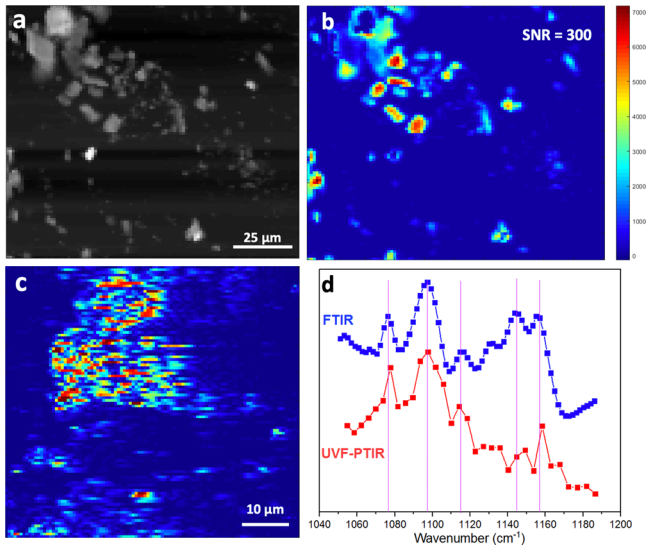

Figure 2. (a) Epi-fluorescence image of silica gel particles with R6G used as the F-PTIR reporter. (b) F-PTIR image of the same FOV, demonstrating an SNR of 300. (c) Label-free UVF-PTIR image of tryptophan microcrystals. (d) Recovered UVF-PTIR spectrum of tryptophan in comparison with FTIR spectrum.

Images acquired with all 32 QCL channels active produced an SNR of 300 for a modulation depth around 10%. This SNR is within a factor of 2 of the theoretical maximum shot-noise limited SNR based on measurements of the fluorescence photon flux. Image edge analysis yielded an upper bound for the spatial resolution of 1.7 μm by F-PTIR, which is just slightly below the resolution recovered by analogous analysis of the epi-fluorescence (1.0 μm).

Label-free ultraviolet F-PTIR (UVF-PTIR) measurements based on two-photon excited intrinsic autofluorescence are shown in Figure 2C,D for tryptophan and in the Supporting Information for lyophilized lysozyme particles. The infrared spectroscopy agreed well with bulk absorption measurements.

https://doi.org/10.1021/jacs.1c03269
J. Am. Chem. Soc. 2021, 143, 10809−10815

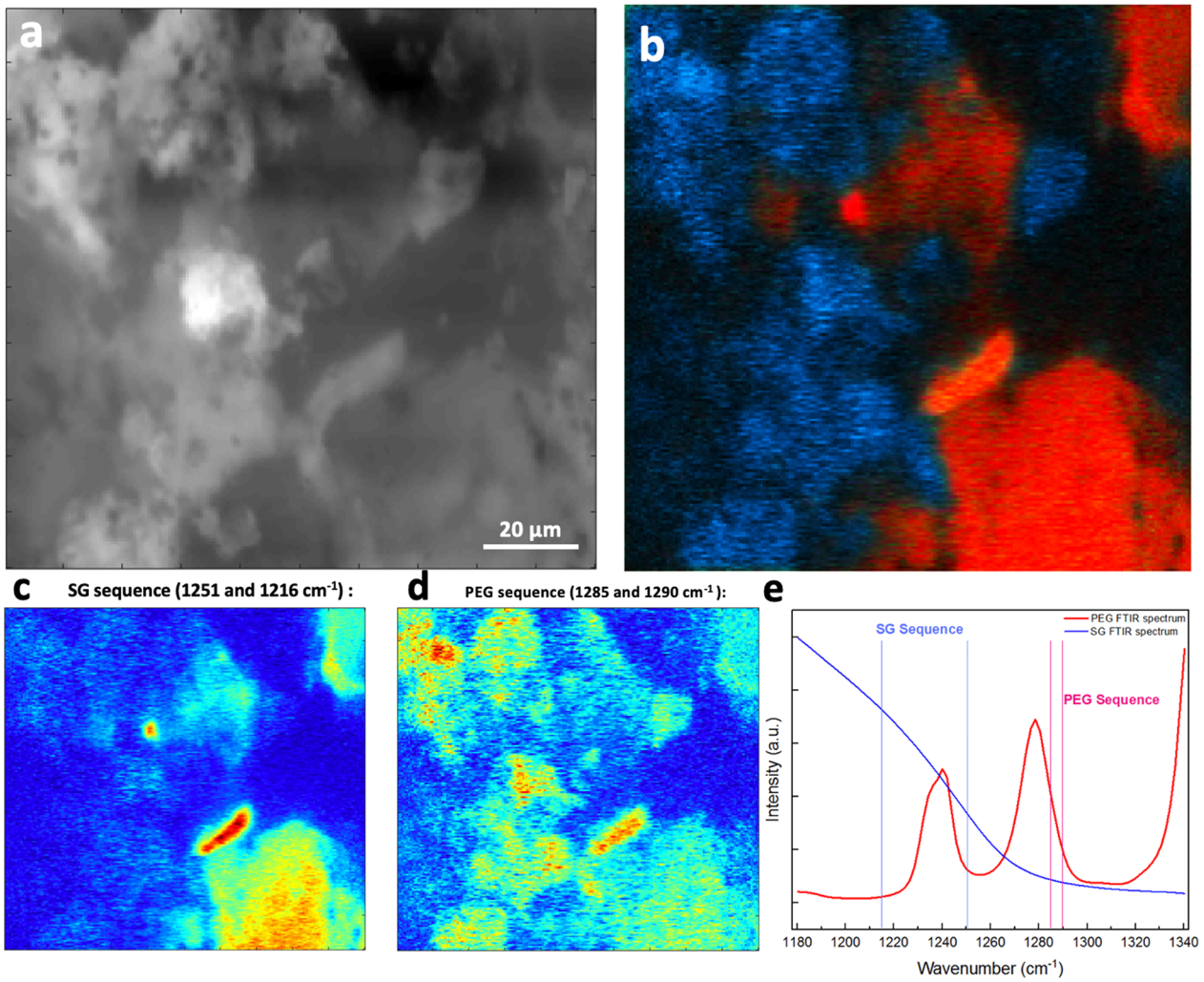

Figure 3. F-PTIR microscopy of a mixture of R6G-associated silica gel (SG) and PEG particles. (a) Epi-fluorescence image of the FOV. (b) Components map within the FOV following spectral decomposition. Red regions correspond to species identified as SG; blue regions correspond to PEG. (c and d) Raw F-PTIR images collected while operating the QCL at off- and on-resonance wavenumbers for PEG. (e) FTIR spectra of the components with vertical lines corresponding to spectral channels used in QCL sequences.

Illustrated in Figure 3A, microscopy measurements were next performed to spectroscopically discriminate between particles in a mixture of two powdered materials: PEG and hydrated silica gel. From initial measurements of the unprocessed F-PTIR spectra of each of the two isolated materials, a compressive sensing binary wavelength mask was calculated to optimally discriminate between the two particles (detailed in the Supporting Information).[31] Following this calculation, F-PTIR microscopy measurements were performed serially using two 2-channel mask patterns optimized to resolve PEG and silica gel particles (Figure 3B). Consistent with these mask designs, images using QCL channels spectrally optimized for each component exhibited little cross-talk and allowed for clear identification of the composition of individual particles (Figure 3C−E) following spectral demixing.

Building on the results of these proof-of-concept studies with known materials, F-PTIR images of amorphous solid dispersions of ritonavir in PVPVA were acquired to explore the possible generation of amorphous phase-separated ritonavir-rich domains. Amorphous solid dispersions are widely used to address low aqueous solubility limitations of many active pharmaceutical ingredients (APIs) by dispersing the API within a polymer with established dissolution properties. In typical use cases, dissolution of the polymer results in release of the API according to kinetics dictated by the polymer rather than the solid-state form of the API. However, prior studies of numerous ASD formulations have reported a "dropping off a cliff" phenomenon, shown in Figure 4A, in which API-loadings higher than a critical threshold result in abrupt *reductions* in the rate or extent of API dissolution.[32,33]

We conjecture that this reduction may be a consequence of phase separation and the formation of API-rich domains of low aqueous solubility. Building on our prior work,[34] spin-case films of ritonavir in PVPVA with trace (0.1%) Nile red added as a fluorescence reporter were exposed to high humidity for 1 h to induce phase separation and then F-PTIR measured to determine composition within the phase-separated domains (Figure 4C and D).

From the results of the F-PTIR measurements, phase-separated domains exhibit clear enrichment in ritonavir based on the mid-infrared spectroscopy. To further corroborate the F-PTIR measurements and to assess the possible perturbation by the fluorescent marker, complementary label-free measurements of ritonavir/PVPVA mixtures were recorded by two-

https://doi.org/10.1021/jacs.1c03269
J. Am. Chem. Soc. 2021, 143, 10809−10815

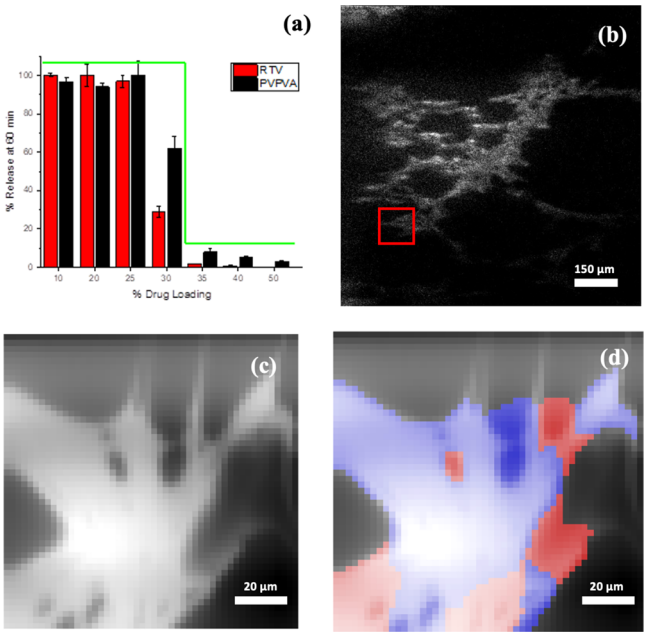

Figure 4. F-PTIR microscopy of amorphous phase-separated ritonavir/PVPVA dispersions. (a) Illustration of the "dropping off a cliff" release phenomenon.[33] (b) Label-free TPE-UVF images of the phase-separated film. The red boxed region illustrates the size of the FOV used for F-PTIR. (c) Epi-fluorescence image of the FOV used for F-PTIR measurements, with Nile Red partitioning to the bright domains. (d) Classification of ritonavir-rich (blue) and PVPVA-rich (red) domains based on F-PTIR results. The image was segmented into 27 "superpixels" and each of them was assigned to either one of the components or background (see SI).

photon excited ultraviolet fluorescence (TPE-UVF) images, shown in Figure 4B over a larger field of view. TPE-UVF leverages the weak but nonzero autofluorescence of ritonavir as an image contrast agent.[35] Comparisons of Figure 4B and 4D indicate clear structural similarities between the phase-separated domains corresponding to ritonavir as identified by F-PTIR spectroscopy with those producing native TPE-UVF in the absence of a fluorescent marker.

Spatial Fourier transform fluorescence recovery after photobleaching experiments (FT-FRAP) following Geiger et al.[36] confirm fluidity within the two phase-separated domains, with ~3-fold lower viscosity within the brightly fluorescent domains (see Supporting Information for details).

Collectively, these results provide compelling evidence supporting amorphous/amorphous phase separation of API-rich domains within ritonavir/PVPVA films upon water uptake. These microscopic chemical microscopy measurements by F-PTIR further support an important role of liquid/liquid phase separation in dictating the kinetics of API dissolution from ASDs that determine bioavailability.

The initial demonstration of F-PTIR herein lays a foundation to couple a diverse suite of fluorescence-based sensing strategies for signal transduction of mid-infrared absorption. Most directly, fluorescence provides specificity to labeled structures interrogated by IR absorption through F-PTIR; the fluorophore must reside within the thermal plume of the IR absorber in order to register a photothermal perturbation. The higher sensitivity of F-PTIR relative to O-PTIR suggests potential greater ease of integration into wide-field PTIR microscopy measurements. Furthermore, super-localization of fluorescence through STORM/PALM approaches can routinely yield spatial resolution on the order of tens of nanometers in bulk media, suggesting potential promise for performing infrared spectroscopy by F-PTIR localized in 3D at comparable spatial resolution.

■ ASSOCIATED CONTENT

Supporting Information

The Supporting Information is available free of charge at https://pubs.acs.org/doi/10.1021/jacs.1c03269.

QCL specification and timing description; measurements of the copropagating beam profile; F-PTIR microscope resolution determination; non-negative matrix factorization operation for optimizing the concentration map of silica gel and PEG; PVPVA – ritonavir phase-separated sample preparation; description of the superpixel segmentation method for phase-separated sample; FRAP analysis of viscosity differences between the phase-separated domains; and simulation details and results. (PDF)

■ AUTHOR INFORMATION

Corresponding Author

Garth J. Simpson – *Department of Chemistry, Purdue University, West Lafayette, Indiana 47907, United States;* orcid.org/0000-0002-3932-848X; Email: gsimpson@purdue.edu

Authors

Minghe Li – *Department of Chemistry, Purdue University, West Lafayette, Indiana 47907, United States*

Aleksandr Razumtcev – *Department of Chemistry, Purdue University, West Lafayette, Indiana 47907, United States*

Ruochen Yang – *Physical and Industrial Pharmacy, Purdue University, West Lafayette, Indiana 47907, United States*

Youlin Liu – *Department of Chemistry, Purdue University, West Lafayette, Indiana 47907, United States*

Jiayue Rong – *Department of Chemistry, Purdue University, West Lafayette, Indiana 47907, United States*

Andreas C. Geiger – *Department of Chemistry, Purdue University, West Lafayette, Indiana 47907, United States;* orcid.org/0000-0002-0472-6648

Romain Blanchard – *Pendar Technologies, Cambridge, Massachusetts 02138, United States*

Christian Pfluegl – *Pendar Technologies, Cambridge, Massachusetts 02138, United States*

Lynne S. Taylor – *Physical and Industrial Pharmacy, Purdue University, West Lafayette, Indiana 47907, United States;* orcid.org/0000-0002-4568-6021

Complete contact information is available at: https://pubs.acs.org/10.1021/jacs.1c03269

Author Contributions

‖M.L. and A.R. contributed equally.

Notes

The authors declare the following competing financial interest(s): R.B. and C.P. work at a company "Pendar Technologies" that incorporates the QCL into commercial products.

■ ACKNOWLEDGMENTS

M.L., A.R., and G.J.S. gratefully acknowledge funding from the National Science Foundation (GOALI-CHE-1710475, NSF-D3SC-2004046, and CIF-1763896). M.L. and A.R. also acknowledge support from the NSF Center for Bioanalytic Metrology (IIP-1916691). R.Y. acknowledges the Agency for Science, Technology and Research (A*STAR), Singapore for funding. Pendar Technologies acknowledges support from the US Army under SBIR Topic A14A-T015.

■ REFERENCES

(1) Dazzi, A.; Prazeres, R.; Glotin, E.; Ortega, J. M. Local infrared microspectroscopy with subwavelength spatial resolution with an atomic force microscope tip used as a photothermal sensor. *Opt. Lett.* **2005**, *30* (18), 2388−2390.
(2) Dazzi, A.; Glotin, F.; Carminati, R. Theory of infrared nanospectroscopy by photothermal induced resonance. *J. Appl. Phys.* **2010**, *107* (12), 124519.
(3) Centrone, A. Infrared Imaging and Spectroscopy Beyond the Diffraction Limit. In *Annual Review of Analytical Chemistry, Vol. 8*; Cooks, R. G., Pemberton, J. E., Eds.; 2015; Vol. *8*, pp 101−126.
(4) Li, N.; Taylor, L. S. Nanoscale Infrared, Thermal, and Mechanical Characterization of Telaprevir-Polymer Miscibility in Amorphous Solid Dispersions Prepared by Solvent Evaporation. *Mol. Pharmaceutics* **2016**, *13* (3), 1123−1136.
(5) Zhang, D. L.; Li, C.; Zhang, C.; Slipchenko, M. N.; Eakins, G.; Cheng, J. X. Depth-resolved mid-infrared photothermal imaging of living cells and organisms with submicrometer spatial resolution. *Sci. Adv.* **2016**, *2* (9), e1600521.
(6) Lee, E. S.; Lee, J. Y. High resolution cellular imaging with nonlinear optical infrared microscopy. *Opt. Express* **2011**, *19* (2), 1378−1384.
(7) Li, C.; Zhang, D. L.; Slipchenko, M. N.; Cheng, J. X. Mid-Infrared Photothermal Imaging of Active Pharmaceutical Ingredients at Submicrometer Spatial Resolution. *Anal. Chem.* **2017**, *89* (9), 4863−4867.
(8) Hawkes, J. B.; Astheimer, R. W. The Temperature Coefficient of the Refractive Index of Water. *J. Opt. Soc. Am.* **1948**, *38* (9), 804−806.
(9) Tokeshi, M.; Uchida, M.; Hibara, A.; Sawada, T.; Kitamori, T. Determination of Subyoctomole Amounts of Nonfluorescent Molecules Using a Thermal Lens Microscope: Subsingle-Molecule Determination. *Anal. Chem.* **2001**, *73* (9), 2112−2116.
(10) Snook, R. D.; Lowe, R. D. Thermal lens spectrometry. *Analyst* **1995**, *120* (8), 2051−2068.
(11) Wallace, W. E. *NIST Chemistry WebBook*, NIST Standard Reference Database Number 69.
(12) Wang, Z.; Millet, L.; Mir, M.; Ding, H. F.; Unarunotai, S.; Rogers, J.; Gillette, M. U.; Popescu, G. Spatial light interference microscopy (SLIM). *Opt. Express* **2011**, *19* (2), 1016−1026.
(13) Kim, T.; Zhou, R. J.; Mir, M.; Babacan, S. D.; Carney, P. S.; Goddard, L. L.; Popescu, G. White-light diffraction tomography of unlabelled live cells. *Nat. Photonics* **2014**, *8* (3), 256−263.
(14) Park, Y.; Depeursinge, C.; Popescu, G. Quantitative phase imaging in biomedicine. *Nat. Photonics* **2018**, *12* (10), 578−589.
(15) Zhang, D. L.; Lan, L.; Bai, Y. R.; Majeed, H.; Kandel, M. E.; Popescu, G.; Cheng, J. X. Bond-selective transient phase imaging via sensing of the infrared photothermal effect. *Light: Sci. Appl.* **2019**, *8*, 12.
(16) Adhikari, S.; Spaeth, P.; Kar, A.; Baaske, M. D.; Khatua, S.; Orrit, M. Photothermal Microscopy: Imaging the Optical Absorption of Single Nanoparticles and Single Molecules. *ACS Nano* **2020**, *14* (12), 16414−16445.
(17) Wang, X. D.; Wolfbeis, O. S.; Meier, R. J. Luminescent probes and sensors for temperature. *Chem. Soc. Rev.* **2013**, *42* (19), 7834−7869.
(18) Wienken, C. J.; Baaske, P.; Rothbauer, U.; Braun, D.; Duhr, S. Protein-binding assays in biological liquids using microscale thermophoresis. *Nat. Commun.* **2010**, *1*, 100.
(19) Jerabek-Willemsen, M.; Wienken, C. J.; Braun, D.; Baaske, P.; Duhr, S. Molecular Interaction Studies Using Microscale Thermophoresis. *Assay Drug Dev. Technol.* **2011**, *9* (4), 342−353.
(20) Seidel, S. A. I.; Dijkman, P. M.; Lea, W. A.; van den Bogaart, G.; Jerabek-Willemsen, M.; Lazic, A.; Joseph, J. S.; Srinivasan, P.; Baaske, P.; Simeonov, A.; Katritch, I.; Melo, F. A.; Ladbury, J. E.; Schreiber, G.; Watts, A.; Braun, D.; Duhr, S. Microscale thermophoresis quantifies biomolecular interactions under previously challenging conditions. *Methods* **2013**, *59* (3), 301−315.
(21) Jerabek-Willemsen, M.; Andre, T.; Wanner, R.; Roth, H. M.; Duhr, S.; Baaske, P.; Breitsprecher, D. MicroScale Thermophoresis: Interaction analysis and beyond. *J. Mol. Struct.* **2014**, *1077*, 101−113.
(22) Kachlishvili, K.; Dave, K.; Gruebele, M.; Scheraga, H. A.; Maisuradze, G. G. Eliminating a Protein Folding Intermediate by Tuning a Local Hydrophobic Contact. *J. Phys. Chem. B* **2017**, *121* (15), 3276−3284.
(23) Gelman, H.; Wirth, A. J.; Gruebele, M. ReAsH as a Quantitative Probe of In-Cell Protein Dynamics. *Biochemistry* **2016**, *55* (13), 1968−1976.
(24) Chen, T.; Dave, K.; Gruebele, M. Pressure- and heat-induced protein unfolding in bacterial cells: crowding vs. sticking. *FEBS Lett.* **2018**, *592* (8), 1357−1365.
(25) Prigozhin, M. B.; Chao, S. H.; Sukenik, S.; Pogorelov, T. V.; Gruebele, M. Mapping fast protein folding with multiple-site fluorescent probes. *Proc. Natl. Acad. Sci. U. S. A.* **2015**, *112* (26), 7966−7971.
(26) Ross, D.; Gaitan, M.; Locascio, L. E. Temperature measurement in microfluidic systems using a temperature-dependent fluorescent dye. *Anal. Chem.* **2001**, *73* (17), 4117−4123.
(27) Whaley-Mayda, L.; Guha, A.; Penwell, S. B.; Tokmakoff, A. Fluorescence-Encoded Infrared Vibrational Spectroscopy with Single-Molecule Sensitivity. *J. Am. Chem. Soc.* **2021**, *143* (8), 3060−3064.
(28) Gonzalez, C.; Iglesias, M.; Lanz, J.; Marino, G.; Orge, B.; Resa, J. M. Temperature influence on refractive indices and isentropic compressibilities of alcohol (C-2-C-4)+olive oil mixtures. *J. Food Eng.* **2001**, *50* (1), 29−40.
(29) Dobbins, H. M.; Peck, E. R. Change of Refractive-Index of Water as a Function of Temperature. *J. Opt. Soc. Am.* **1973**, *63* (3), 318−320.
(30) Liao, C. S.; Blanchard, R.; Pfluegl, C.; Azimi, M.; Huettig, F.; Vakhshoori, D. Portable broadband photoacoustic spectroscopy for trace gas detection by quantum cascade laser arrays. *Opt. Lett.* **2020**, *45* (12), 3248−3251.
(31) Rehrauer, O. G.; Dinh, V. C.; Mankani, B. R.; Buzzard, G. T.; Lucier, B. J.; Ben-Amotz, D. Binary Complementary Filters for Compressive Raman Spectroscopy. *Appl. Spectrosc.* **2018**, *72* (1), 69−78.
(32) Saboo, S.; Moseson, D. E.; Kestur, U. S.; Taylor, L. S. Patterns of drug release as a function of drug loading from amorphous solid dispersions: A comparison of five different polymers. *Eur. J. Pharm. Sci.* **2020**, *155*, 105514.
(33) Indulkar, A. S.; Lou, X. C.; Zhang, G. G. Z.; Taylor, L. S. Insights into the Dissolution Mechanism of Ritonavir-Copovidone Amorphous Solid Dispersions: Importance of Congruent Release for Enhanced Performance. *Mol. Pharmaceutics* **2019**, *16* (3), 1327−1339.
(34) Li, N.; Cape, J. L.; Mankani, B. R.; Zemlyanov, D. Y.; Shepard, K. B.; Morgen, M. M.; Taylor, L. S. Water-Induced Phase Separation of Spray-Dried Amorphous Solid Dispersions. *Mol. Pharmaceutics* **2020**, *17* (10), 4004−4017.
(35) Toth, S. J.; Madden, J. T.; Taylor, L. S.; Marsac, P.; Simpson, G. J. Selective Imaging of Active Pharmaceutical Ingredients in Powdered Blends with Common Excipients Utilizing Two-Photon Excited Ultraviolet-Fluorescence and Ultraviolet-Second Order Nonlinear Optical Imaging of Chiral Crystals. *Anal. Chem.* **2012**, *84* (14), 5869−5875.

https://doi.org/10.1021/jacs.1c03269
J. Am. Chem. Soc. 2021, 143, 10809−10815

(36) Geiger, A. C.; Smith, C. J.; Takanti, N.; Harmon, D. M.; Carlsen, M. S.; Simpson, G. J. Anomalous Diffusion Characterization by Fourier Transform-FRAP with Patterned Illumination. *Biophys. J.* **2020**, *119* (4), 737−748.

https://doi.org/10.1021/jacs.1c03269
J. Am. Chem. Soc. 2021, 143, 10809−10815